Coupling of sausage, kink, and magneto-Rayleigh-Taylor instabilities in a cylindrical liner

M. R. Weis,[1] P. Zhang,[1] Y. Y. Lau,[1,a)] P. F. Schmit,[2] K. J. Peterson,[2] M. Hess,[2] and R. M. Gilgenbach[1]
[1]*Department of Nuclear Engineering and Radiological Sciences, University of Michigan, Ann Arbor, Michigan 48109-2104, USA*
[2]*Sandia National Laboratories, Albuquerque, New Mexico 87185, USA*

(Received 20 January 2015; accepted 5 March 2015; published online 24 March 2015)

This paper analyzes the coupling of magneto-Rayleigh-Taylor (MRT), sausage, and kink modes in an imploding cylindrical liner, using ideal MHD. A uniform axial magnetic field of arbitrary value is included in each region: liner, its interior, and its exterior. The dispersion relation is solved exactly, for arbitrary radial acceleration ($-g$), axial wavenumber (k), azimuthal mode number (m), liner aspect ratio, and equilibrium quantities in each region. For small k, a positive g (inward radial acceleration in the lab frame) tends to stabilize the sausage mode, but destabilize the kink mode. For large k, a positive g destabilizes both the kink and sausage mode. Using the 1D-HYDRA simulation results for an equilibrium model that includes a pre-existing axial magnetic field and a pre-heated fuel, we identify several stages of MRT-sausage-kink mode evolution. We find that the $m = 1$ kink-MRT mode has a higher growth rate at the initial stage and stagnation stage of the implosion, and that the $m = 0$ sausage-MRT mode dominates at the main part of implosion. This analysis also sheds light on a puzzling feature in Harris' classic paper of MRT [E. G. Harris, Phys. Fluids **5**, 1057 (1962)]. An attempt is made to interpret the persistence of the observed helical structures [Awe *et al.*, Phys. Rev. Lett. **111**, 235005 (2013)] in terms of non-axisymmetric eigenmode.
 [http://dx.doi.org/10.1063/1.4915520]

I. INTRODUCTION

When a strong axial current is present, the dominant instabilities on a cylindrical plasma column are the sausage and kink mode, with azimuthal mode numbers, $m = 0$ and $m = 1$, respectively. If the plasma column is in the form of a cylindrical liner of outer radius R and thickness Δ, the sausage and kink mode are still the dominant modes if it is assumed that there is a sufficient internal pressure in the central region of the liner to prevent any radial acceleration of the liner. However, if this internal pressure is weak, there would be inward acceleration of the liner, and the outer interface of the liner would be subjected to the magneto-Rayleigh-Taylor instability (MRT).[1–5] If, on the other hand, the internal pressure in the central region is very high, there is a radially outward acceleration and the inner interface of the cylindrical liner would be subjected to MRT. In the rest frame of the interface, the effective gravity, g, is equal to the negative of the radial acceleration. Thus, $g > 0$ ($g < 0$) corresponds to implosion (stagnation or explosion), and the conventional sausage and kink mode described above correspond to $g = 0$. It is clear that the nature of sausage, kink, MRT, and the coupling among them depends much on the cylindrical geometry, on the magnitude and sign of g, on the aspect ratio, R/Δ, and on the dominant magnetic field. In this paper, we use the ideal MHD model and present a general linear stability analysis including the $m = 0$ MRT-sausage mode and the $m = 1$ MRT-kink mode, for arbitrary value (and sign) of g, for arbitrary aspect ratio R/Δ (>1), and for general values of the axial magnetic field outside, inside, and within the liner.

The coupling of the $m = 0$ MRT and sausage mode, and the coupling of the $m = 1$ MRT and kink mode, has received only scant attention in the past.[4–7] They have become an important issue in the recent magnetized liner inertial fusion (MagLIF) experiments[8–14] on the Z-machine at Sandia National Laboratories. While there have been extensive studies of MRT on the MagLIF liner without an axial magnetic field,[9–11] many of these MRT theories were based on a slab geometry which is incapable of describing the conventional sausage mode and kink mode.[2–4,15–18] Without an axial magnetic field, MRT structure is typically oriented along nearly horizontal planes perpendicular to the z-axis with limited or no pitch.[12,13] However, with the inclusion of an axial magnetic field, helical structures were found with significant inclination during the implosion phase.[12,13] In the fully integrated MagLIF experiments (with axial magnetic field and a preheated fuel in the central region inside the liner), possible kink-like perturbations of the plasma column were reported at stagnation.[14] These non-axisymmetric MHD activities are yet to be explained.

To keep the problem analytically tractable, we use ideal MHD and apply a linear stability analysis on a sharp boundary model (Fig. 1). For the linear stability analysis, we assume (a) that the liner has a uniform and constant density, the density elsewhere is practically zero in comparison, (b) that there is a constant, uniform axial magnetic field in each region, (c) that the azimuthal magnetic field, generated by

a)Corresponding author: yylau@umich.edu

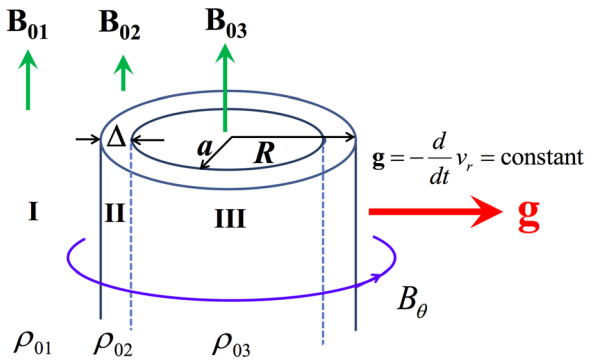

FIG. 1. MHD model for an imploding cylindrical liner. Uniform axial magnetic field is included in each region: liner ($a < r < R$), its interior ($r < a$), and its exterior ($r > R$), as B_{02}, B_{03}, and B_{01}, respectively.

the axial current (a surface current), exists only in the exterior region ($r > R$), (d) that R and Δ are constants, and (e) that the effective gravity, g, is uniform and constant. These assumptions may be justified if we pretend that the liner is subjected to an instantaneous, initial inward acceleration ($= -g$), so that the MRT mechanism is switched on, but without creating any motion of the liner so that R, Δ, and the liner density are essentially constants. Such a simplified conceptual model enables a close examination of the relation between a purely MRT mode (one without any internal pressure to reduce the acceleration), and a purely sausage and kink mode (one with $g = 0$). In so doing, we are able to resolve a little-noted puzzle in Harris' classic paper which shows that there is a finite MRT growth rate, $\gamma = \sqrt{g/R}$, for a thin shell even when $k = m = 0$, where R is the radius of the thin shell and k is the axial wavenumber of the imploding thin liner.[4] This is a surprising result because the MRT growth rate is expected to be $\gamma = \sqrt{(k_\theta^2 + k_z^2)^{1/2} g}$, and for m and k equal to zero, we would have $\gamma = 0$. The nature of this finite growth rate of Harris and its relation to the $m = 0$ sausage mode will be discussed.

In experiments, the axial current has a finite rise time. Quantities such as the outer radius R, and g will then evolve in time. In fact, the effective gravity g even changes sign from implosion to stagnation. To obtain some rough understanding of the relative importance of MRT, sausage, and kink, on a liner like MagLIF, we use the HYDRA simulation code[19] to examine the temporal evolution of a cylindrical liner with a realistic current rise profile reaching ~20 MA in 150 ns, a pre-seeded axial magnetic field of 10 T, and a preheated fuel (~250 eV), similar to an ideal version of the fully integrated MagLIF experiments by Gomez *et al.*[14] From 1D HYDRA simulations, we extract the instantaneous "equilibrium" parameters for R, Δ, g, B_θ, B_{03}, etc., and apply these profiles to the linear stability theory of the sharp boundary model. This analysis, reported below, reveals several stages of evolution of sausage, kink, and MRT, from implosion to stagnation. Figure 5 below illustrates the relative importance of the $m = 0$ and $m = 1$ modes at the different stages.

We shall first consider the equilibrium model (Fig. 1), in which the internal pressure in each region is assumed to be adjusted so that g may be assigned an arbitrary constant value (zero, positive, or negative), for a given set of axial and azimuthal magnetic fields. The results of the stability analysis for general m and k are presented. Numerical results are presented only for the $m = 0$ and $m = 1$ modes.

II. EQUILIBRIUM AND STABILITY

The model under study is shown in Fig. 1. It consists of three regions, I, II, and III. In each region, we assume that the fluid is perfectly conducting. We solve the ideal MHD equations: $\rho(\partial/\partial t + \mathbf{v}\cdot\nabla)\mathbf{v} = -\nabla p + \mathbf{J}\times\mathbf{B} + \rho g\mathbf{r}$, $\partial\rho/\partial t + \nabla\cdot(\rho\mathbf{v}) = 0$, $\partial\mathbf{B}/\partial t = \nabla\times(\mathbf{v}\times\mathbf{B})$, and $\nabla\times\mathbf{B} = \mu_0\mathbf{J}$ in the cylindrical coordinates. Here, ρ is the mass density, $\mathbf{v}$ is the fluid velocity, p is the fluid pressure which is assumed to be isotropic, $\mathbf{J}$ is the current density, $\mathbf{B}$ is the magnetic field, g is the gravity which is positive when acceleration is radially inward [Fig. 1], $\mathbf{r}$ is the unit radial vector, and μ_0 is the free space permeability.

In equilibrium, the magnetic field in the three regions, I ($r > R$), II ($a < r < R$), and III ($r < a$) is assumed to be, respectively, $\mathbf{B_{01}} = \mathbf{z}B_{01} + \boldsymbol{\theta}B_\theta R/r$, $\mathbf{B_{02}} = \mathbf{z}B_{02}$, and $\mathbf{B_{03}} = \mathbf{z}B_{03}$, where B_{01}, B_{02}, B_{03}, and B_θ are constants. We further assume that the mass density in each region is also constant with the liner density being the dominant, i.e., $\rho_{01} \ll \rho_{02}$, and $\rho_{03} \ll \rho_{02}$. For a scenario such as MagLIF, region I is a vacuum field region, region II is the liner region, and region III is the fuel region. The equilibrium pressure profile p_0(r) is adjusted so that it satisfies the equilibrium condition,[20] for all r,

$$\frac{\partial}{\partial r}\left(p_0(r) + \frac{B_0^2(r)}{2\mu_0}\right) + \frac{B_{0\theta}^2(r)}{r\mu_0} = \rho_0(r)g, \tag{1}$$

where $B_0 = |\mathbf{B_0}|$ is the magnitude of the equilibrium magnetic field $\mathbf{B_0}$ and $B_{0\theta}(r)$ is the azimuthal component of $\mathbf{B_0}$. We assume that the effective gravity, g, is a constant, though fully incompressible flow would require a non-uniform g to account for cylindrical convergence and mass conservation consistently. This may be justified if we use 1D HYDRA simulations to provide these equilibrium profiles, which fully take into account compressibility of the fluid as it implodes. Also, the thickness of the shell remains on the order of 100s of micrometers, which is relatively thin so that the effect of non-uniform g remains small. Integrate Eq. (1) across region II to yield

$$g\rho_{02}\Delta = \left[p_I + \frac{B_{01}^2 + B_\theta^2}{2\mu_0}\right] - \left[p_{III} + \frac{B_{03}^2}{2\mu_0}\right], \tag{2}$$

where $\Delta = R - a$ is the liner thickness, p_I is the equilibrium fluid pressure in region I at the outer liner surface, and p_{III} is the equilibrium fluid pressure in region III at the inner liner surface. The acceleration, which equals $-g$, may therefore be driven by an arbitrary mix of fluid pressure (p_{III}, p_I) or magnetic pressure (B_{01}, B_{03}, B_θ), as long as the above equilibrium conditions are satisfied. Note that if the internal pressure p_{III} is dominant among all pressures, as in the stagnation stage, then g is negative (acceleration is radially outward) in Eq. (2). Hereafter, we will call the case $g = 0$ pure kink mode and pure sausage mode, i.e., the total pressure exactly balances when there is no acceleration in the laboratory frame. On the other hand, if one square bracket in

Eq. (2) is much larger than the other square bracket, so that $|g|$ is maximized, we call the unstable mode pure MRT or pure RT mode. In general, $|g|$ is between zero and its maximum value; and the resulting instability is somewhere between a pure sausage (or kink) mode and a pure MRT mode.

We next consider a small signal perturbation of the form, $u_1(r)e^{i\omega t+im\theta-ikz}$, on the equilibrium of the 3-region geometry shown in Fig. 1 and assume these perturbations to be incompressible ($\nabla\cdot\mathbf{v}=0$). For the above sharp boundary model, the linearized MHD equations for each region may be distilled into a second order ODE for the perturbed displacement of the plasma, the solution of which requires two boundary conditions, plus constraint on the perturbed magnetic field: (1) A perfect conductor (ideal MHD) requires that the magnetic field component normal to the liner surface to be identically zero, which links the perturbation magnetic field and displacement and (2) The continuity of total pressure across each interface. This leads to a dispersion relation of the form,

$$A\omega^4 - B\omega^2 + C = 0, \tag{3}$$

$$A = (X_1X_2+1)/(X_3^2k^2aR), \tag{4}$$

$$B = b_1 + b_2, \tag{5}$$

$$C = k^2V_{02}^2(k^2V_{02}^2A + b_2) + k^2V_{03}^2(I_{|m|}/I'_{|m|})(-k^2V_{02}^2X_2/X_3 + |k|g') + k^2gg'. \tag{6}$$

In Eqs. (4)–(6), $X_1 = K_{|m|}\hat{I}'_{|m|} - I_{|m|}\hat{K}'_{|m|}$, $X_2 = \hat{I}_{|m|}K'_{|m|} - \hat{K}_{|m|}I'_{|m|}$, $X_3 = \hat{I}'_{|m|}K'_{|m|} - \hat{K}'_{|m|}I'_{|m|}$, $I_{|m|} = I_{|m|}(|k|a)$, $K_{|m|} = K_{|m|}(|k|a)$, $\hat{I}_{|m|} = I_{|m|}(|k|R)$, $\hat{K}_{|m|} = K_{|m|}(|k|R)$, $b_1 = 2k^2V_{02}^2A$, $b_2 = -[(X_1/X_3)|k|g' + (X_2/X_3)|k|g]$, $V_{02} = \sqrt{B_{02}^2/\mu_0\rho_{02}}$, $V_{03} = \sqrt{B_{03}^2/\mu_0\rho_{02}}$, $g' = g + (1/\mu_0\rho_{02}R)\ [B_\theta^2 + (\hat{K}_{|m|}/\hat{K}'_{|m|}|k|R)(-mB_\theta + kRB_{01})^2]$, I_m and K_m are, respectively, the modified Bessel function of order m of the first and second kind, and a prime denotes differentiation of these modified Bessel functions with respect to their arguments. Of the four eigenvalues of ω in the dispersion relation (3), we shall henceforth consider only the most unstable mode with the largest negative imaginary part of ω. This is the exponentially growing mode, the second root is exponentially decaying and the 3rd and 4th are purely oscillatory. The numerical values of the growth rate, obtained from Eq. (3), are presented below. They have all been validated with an independent, alternative approach that directly solved the governing differential equation including $\rho_{03}>0$.

III. m = 0 AND m = 1 MODE WITH g = 0 AND NONZERO g

The difference between a pure sausage mode, and a pure MRT mode, both with $m=0$, is shown in Fig. 2(a), where we have set the axial magnetic field equal to zero everywhere. We further assume that $p_I=0$, and Eq. (2) then reads,

$$g\rho_{02}\Delta = \frac{B_\theta^2}{2\mu_0} - p_{III}. \tag{7}$$

For the pure sausage mode, we set $p_{III} = B_\theta^2/2\mu_0$, so that $g=0$. The normalized growth rate of this pure sausage mode is plotted by the solid lines in Fig. 2(a) for various aspect ratios, from a thin shell ($R/\Delta=10$) to an almost solid cylinder ($R/\Delta=1.0101$). Note that for a thin liner, $R/\Delta\gg1$, the pure sausage mode growth rate, $\gamma=-\mathrm{Im}(\omega)$, approaches the asymptotic limit for small kR,

$$\gamma = \sqrt{\frac{B_\theta^2}{\mu_0\rho_{02}\Delta R}}, \quad \text{pure sausage mode } (kR\ll1, R/\Delta\gg1). \tag{8}$$

Equation (8) may be derived from Eq. (3) in the asymptotic limits shown, after setting $g=0$.

For the pure MRT mode, there is no internal pressure, $p_{III}=0$, in Eq. (7). There is then a maximum inward acceleration, with a maximum $g = g_{\max} = B_\theta^2/2\mu_0\rho_{02}\Delta$ according to Eq. (7). The normalized growth rate for this pure MRT mode with $m=0$ is given by the dashed curves in Fig. 2(a). Asymptotically, one may show from Eq. (3) that, for a thin liner, $R/\Delta\gg1$, and small kR,

$$\gamma = \sqrt{\frac{B_\theta^2}{2\mu_0\rho_{02}\Delta R}}, \quad \text{pure MRT mode } (kR\ll1, R/\Delta\gg1). \tag{9}$$

Equation (9) is identical to Eq. (61) of Harris[4] in the limit $k=0$, $m=0$, thus confirming Harris' finite MRT growth rate in this limit for a collapsing thin shell. Note from Eqs. (8) and (9) that the pure MRT mode has a growth rate lower than the pure sausage mode in the long axial wavelength limit. Since the value of g ranges between $g=0$ and $g=g_{\max}$, we conclude that inward acceleration ($g>0$) tends to stabilize the long wavelength sausage mode, and this is even more apparent in Fig. 2(a) for lower aspect ratios, $R/\Delta=2$, and $R/\Delta=1.0101$. This is also true when $B_{0z}/B_\theta=0.1$, as shown in Fig. 2(c). However, if the axial magnetic field is increased to $B_{0z}/B_\theta=1$ (Fig. 2(e)), the pure sausage mode is stable for all R/Δ, and the inward acceleration destabilizes the pure sausage mode for the $R/\Delta=10$ case (and only for this case among the values of R/Δ shown in Fig. 2(e)). Note that the inward acceleration ($g>0$) tends to destabilize the short wavelength $m=0,1$ modes, when $kR>1$. This result is important when we consider the experiments of Sinars *et al.*[9,10] and simulations and experiments of McBride *et al.*[11] where such modes are observed. They show that while pre-seeded $m=0$ ($k>0$) modes persist, retaining azimuthal symmetry, unmodified liners show a rapid departure from azimuthal symmetry. One explanation with our theory is while the growth rate for $m=0$ ($k>0$) remains the largest, $m>0$ and $k>0$ modes have comparable enough growth rates that, unless preseeded with $m=0$, directly compete and destroy the $m=0$ symmetry. In fact, to accurately simulate a typical unseeded liner, fully 3D modes (m,$k>0$) must be allowed (2D simulations are insufficient), though even this can be challenging[11] and is discussed briefly in the conclusion.

For the kink mode ($m=1$), an inward acceleration ($g>0$) tends to destabilize the kink mode for long axial wavelength ($kR\ll1$), regardless of the value of $B_{0z}/B_{0\theta}=0$, 0.1 or 1, as shown Figs. 2(b), 2(d), and 2(f). The curves with

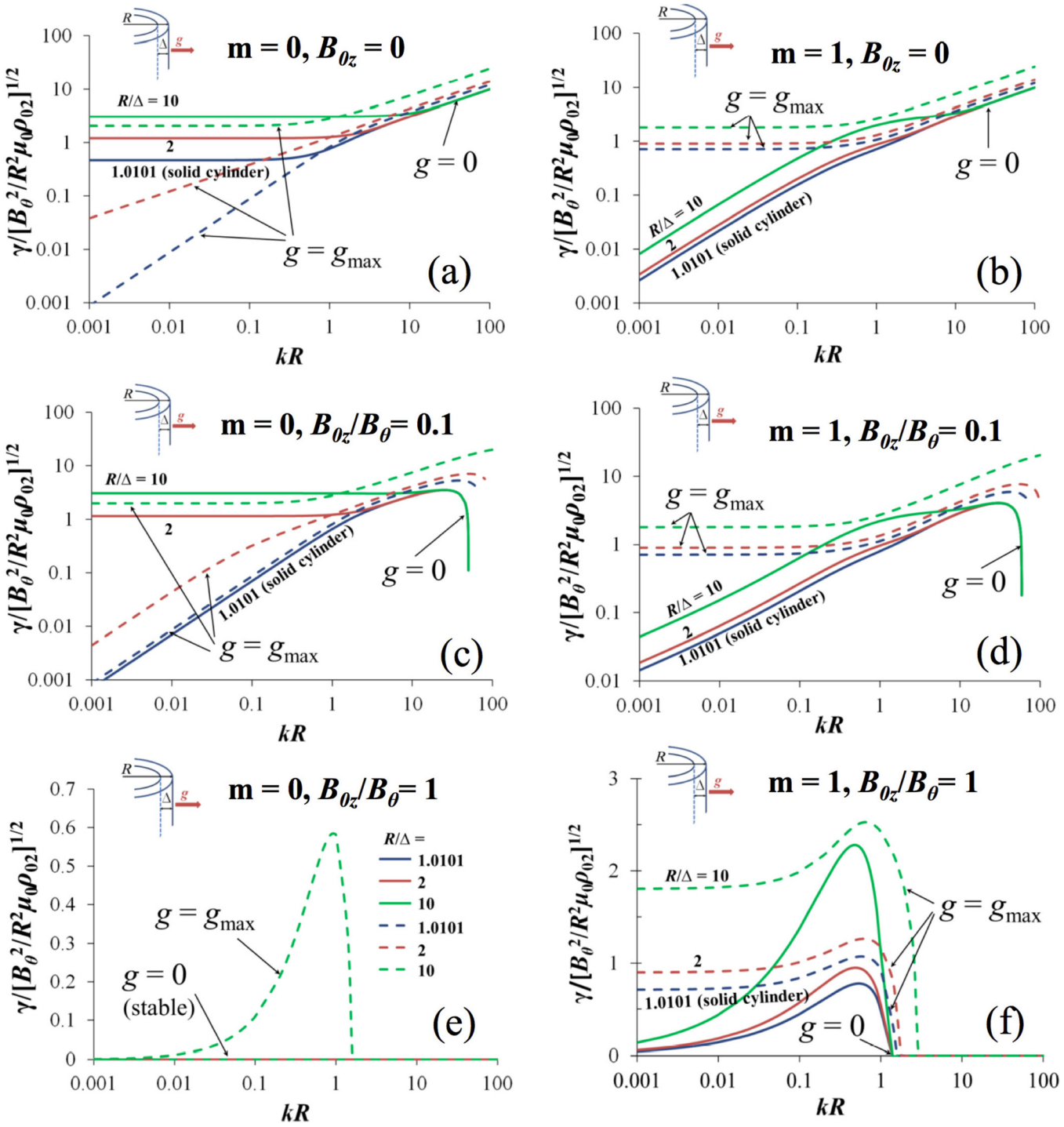

FIG. 2. The normalized growth rate calculated from Eq. (3) for (a), (c), (e), the $m = 0$ mode, and (b), (d), (f), the m = 1 mode, with $B_{0z}/B_\theta = 0$, 0.1, and 1, and $R/\Delta = 1.0101$ (almost a solid cylinder), 2, and 10, where $B_{0z} = B_{01} = B_{02} = B_{03}$. Here, g = 0 corresponds to the pure sausage mode ($m = 0$), or the pure kink mode ($m = 1$), and $g = g_{max} > 0$ corresponds to the pure MRT mode for an imploding liner.

$g = 0$ in Figs. 2(d) and 2(f) show disappearance of $m = 1$ instability for sufficiently large kR. This only means that the Kruskal-Shafranov criterion for kink mode stabilization is satisfied for sufficiently large kR.[20] Note that the inward acceleration ($g > 0$) tends to destabilize the short wavelength $m = 1$ mode, when $kR > 1$.

To gain some understanding of the coupling between MRT, sausage and kink mode at the stagnation stage, we now assume that $B_{01} = B_{02}$ is so small compared with B_{03} that we may now set $B_{01} = B_{02} = 0$. We further assume $B_{03}/B_\theta = 1$. The equilibrium condition, Eq. (2), then reads,

$$g\rho_{02}\Delta = p_I - p_{III}. \tag{10}$$

The pure sausage and pure kink mode assumes $P_I = P_{III}$ so that $g = 0$. Their normalized growth rates are shown by the solid lines in Fig. 3(a) for $m = 0$, and in Fig. 3(b) for $m = 1$. The pure MRT case assumes $P_I = 0$ in Eq. (10), and the normalized growth rates are shown by the dotted lines in Fig. 3,

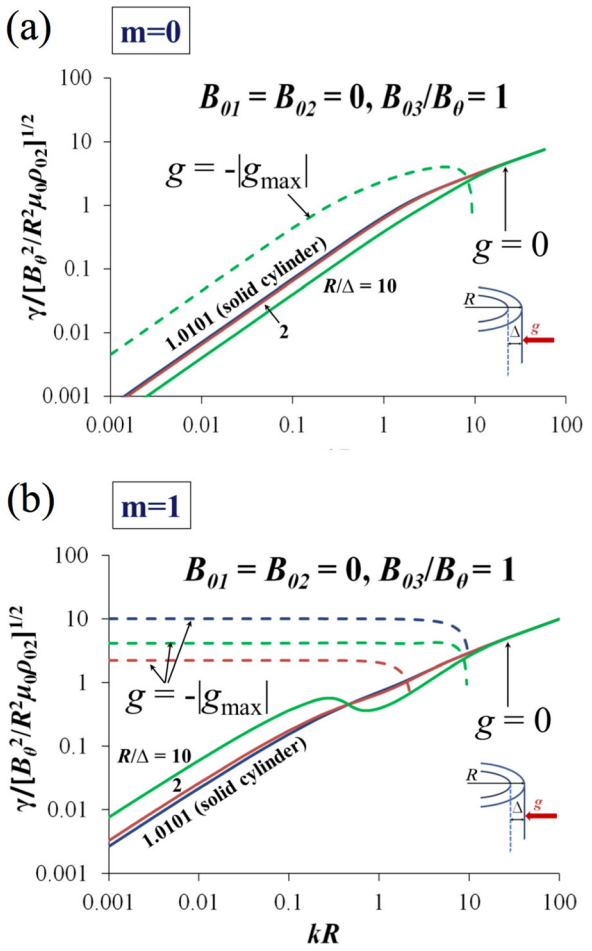

FIG. 3. The normalized growth rate calculated from Eq. (3) for (a), the $m = 0$ mode, and (b), the $m = 1$ mode, with $B_{01} = B_{02} = 0$, and $B_{03}/B_\theta = 1$, for $R/\Delta = 1.0101$ (almost solid cylinder), 2, and 10. Here, $g = 0$ corresponds to the pure sausage mode ($m = 0$), or the pure kink mode ($m = 1$), and $g = -|g_{max}| < 0$ corresponds to the pure MRT mode for an exploding liner near its stagnation.

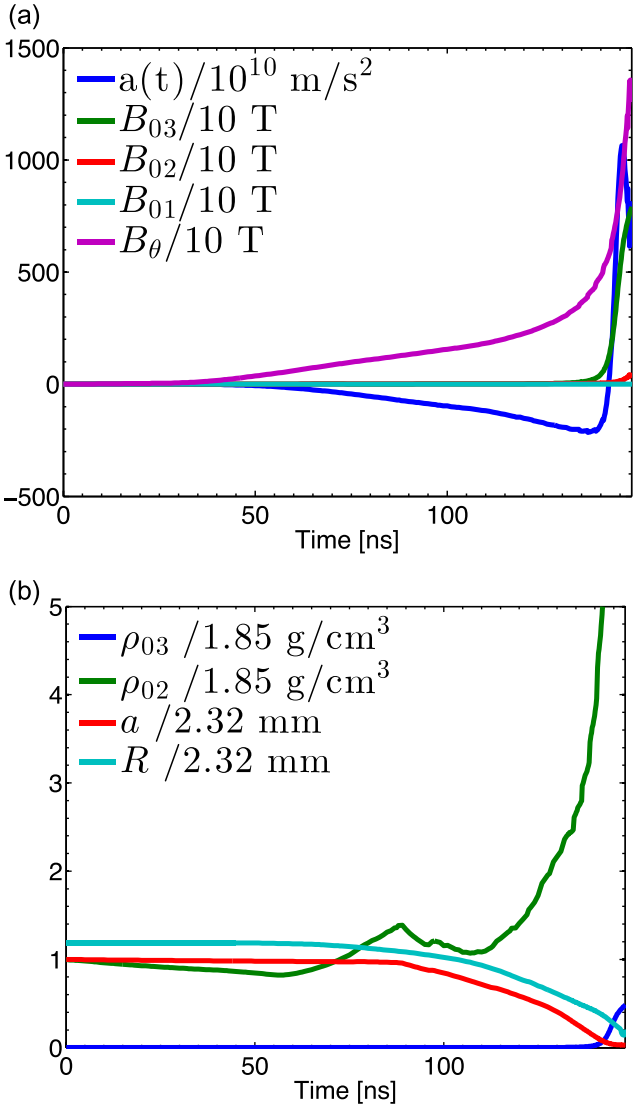

FIG. 4. (a) Evolution of magnetic fields and average liner acceleration, $a = -g$, from 1D HYDRA simulations. (b) Liner trajectory and evolution of the fuel and liner density from 1D HYDRA simulations. At $t = 0$: $B_{01} = B_{02} = B_{03} = 10\,\mathrm{T}$, $B_\theta = 0\,\mathrm{T}$.

where we set $p_{III} = -g_{max}\rho_{02}\Delta = B_\theta^2/\mu_0$. From Fig. 3, we see that the radially outward acceleration ($g < 0$) destabilizes only the thinnest liner for the sausage mode, while all thicknesses are destabilized for the kink mode. Overall, the $m = 1$ MRT mode has a higher growth rate during this deceleration phase with a highly compressed axial field. This may have implications for MagLIF as we will discuss below.

We next calculate the instantaneous instability growth rate for the $m = 0$ and the $m = 1$ modes according to Eq. (3), using the data from 1D HYDRA to obtain the instantaneous equilibrium profiles. The $m = -1$ mode could also be unstable but in general has a smaller growth rate than $m = 0$, 1 so we focus on the more dangerous growth rate. Figure 4 shows the evolution of B_{01}, B_{02}, B_{03}, B_θ, g, R, a, ρ_{02}, and ρ_{03}, for a liner geometry and current profile similar to the fully integrated MagLIF experiments of Gomez *et al.* (with pre-magnetization of a 10 T axial magnetic field, and a preheated fuel[14]). These results are expected to be equally applicable to the experiments of Awe *et al.*,[12,13] except for the deceleration phase since the experiments by Gomez *et al.* included a laser pre-heat. This allows stagnation at smaller convergence ratio, a key feature of MagLIF. Figure 4 was extracted from the HYDRA 1D simulations using the procedure outlined elsewhere.[18] Note from Fig. 4 that during the entire interval of 148 ns, $\rho_{01} = 0$, $\rho_{03} \ll \rho_{02}$ and that $g < 0$ only within the last 7 ns. The instantaneous instability growth rates for the $m = 0$ and the $m = 1$ mode are compared in Fig. 5(a) as a function of time, for various axial wavelengths $\lambda = 2\pi/k$. We interpret Fig. 5(a) as follows, focusing on the $\lambda = 1$ mm case.

For $\lambda = 1$ mm, Fig. 5(a) shows that there are five (5) different stages of MRT-sausage-kink growth for the evolving B_{01}, B_{02}, B_{03}, B_θ, g, R, a, ρ_{02}, and ρ_{03} shown in Fig. 4. (i) Initially, for the first 20 ns, the azimuthal magnetic field is small compared with the pre-seeded axial magnetic field of 10 T, both the $m = 0$ and $m = 1$ modes are stable. (ii) As the azimuthal magnetic field increases, but is still less than the axial magnetic field, the kink mode ($m = 1$) becomes unstable but the sausage mode ($m = 0$) remains stable. This stage is very similar to a tokamak with a safety factor $q < 1$, but will quickly pass. (iii) As the azimuthal magnetic field is increased further, from about 25 to 55 ns, both the kink and

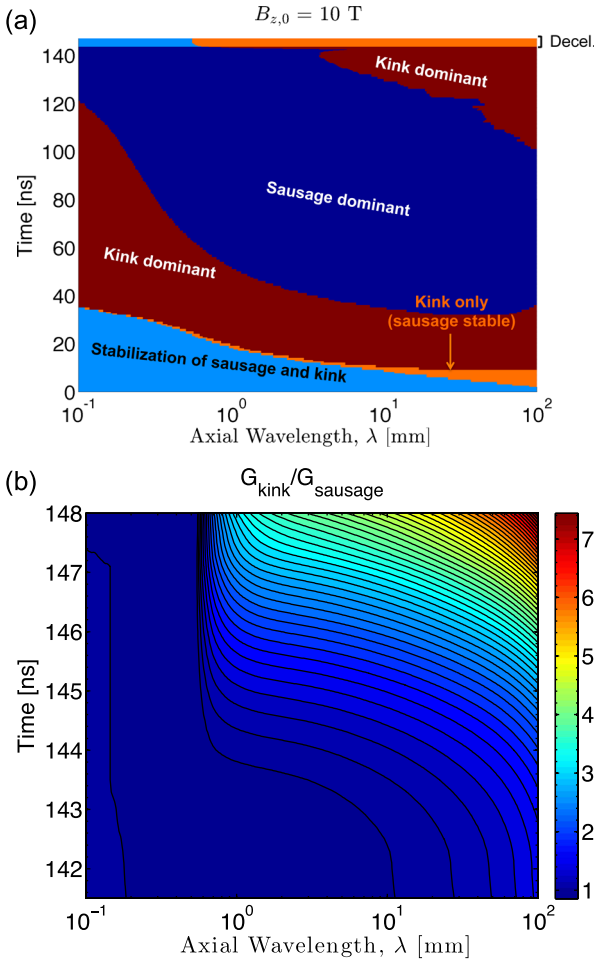

FIG. 5. (a) Relative dominance of sausage and kink modes for a MagLIF like implosion. $g > 0$ up until final 7 ns where it changes sign. Observed experimental axial wavelengths are on the order of 1 mm. (b) Magnification of the last 7 ns, comparing the amplitude gain of the sausage and kink mode as a function of wavelength. Stronger axial fields allow the kink mode to dominate over shorter wavelengths.

sausage mode become unstable, but the kink mode is dominant. This is not the case if there is no axial magnetic field. Thus, the axial magnetic field gives a preference to the growth of the kink mode if helical perturbations are present. One might wonder if the subdominance of the $m = 0$ mode in these early stages has anything to do with the appearance of the helical structures in Awe's experiments.[12,13] Early on, MRT is not important because there is little inward acceleration of the liner (g is small). Over the first 60 ns, the maximum number of e-folds is on the order of 1 for axial wavelengths around 100 μm, while wavelengths on the order of 1 mm have undergone around 0.1 e-folds. Because we use a sharp boundary model, the number of e-folds also depends on the density used. Certainly, there will be some ablation and it is difficult to tell whether the early time growth occurs in the ablated plasma or the bulk, above we have used the near-solid density which may underestimate growth. It is also possible these modes collude with electrothermal instability which tends to occur for short wavelengths ($<$200 μm) at these early times.[21,22] (iv) As the azimuthal magnetic field further increases much beyond the axial magnetic field (from the current rise after 55 ns), both the $m = 0$ and $m = 1$ mode are unstable, but the $m = 0$ mode becomes dominant. At this point g is large, such that MRT is the dominant driver of instability decreasing the e-folding time substantially. This situation remains for the major part of the implosion, all the way until the fuel region is heated up to such a high pressure that the sign of radial acceleration reverses, and the stagnation stage begins. (v) During the deceleration stage (stagnation) in the last 7 ns of the simulation, both the $m = 0$ and $m = 1$ modes are unstable, but the $m = 1$, kink-like mode has a higher total amplitude gain than the $m = 0$ mode during this final stage. Figure 5(b) shows that the kink mode's amplitude gain is about three times that of the sausage mode during this final stage if $\lambda = 1$ mm. Thus, if helical structure has fed-through the liner and seeded the inner surface, this could generate substantial helical growth within the fuel/liner inner surface during the deceleration phase. In fact, from Fig. 3(b), the pure deceleration-MRT $m = 1$ mode exhibits a growth rate with complete lack of dependence on wavelength except for an upper wavenumber cutoff k_{max} (short wavelength). This would suggest that the dominant kink-like perturbation near stagnation will correspond to the most strongly-seeded kink-like liner deformation during run-in.

Finally, we note that the instability growth rates presented above are also in excellent agreement with the benchmark MRT data in Sinars *et al.*[9,10] Experiments showing the growth of seeded $m = 0$, $\lambda_z = 400$ μm modes were presented which also compared very favorably with planar growth rates[10,18] since kR was large. The $m = 0$ modes are fairly straightforward to verify via 2D simulations and also in experiments, however 3D perturbations are much more difficult to investigate. As such, growth rates with $m \neq 0$ and $k \neq 0$ could hopefully be used to benchmark 3D simulation codes, of which there are very few tests.

IV. CONCLUDING REMARKS

This paper concentrates on the cylindrical effects of the stability of a current-carrying liner of various aspect ratios, from a thin liner to a solid cylinder. We focused mainly on the $m = 0$ and $m = 1$ modes and on the effect of radial acceleration on the liner stability. When the radial acceleration is negligible, as is the case during the initial axial current rise, the sausage mode is dominant without an axial magnetic field, but the kink mode is dominant with a pre-seeded axial magnetic field. During the main part of the implosion, the $m = 0$ mode grows faster than the $m = 1$ mode. At the stagnation stage where the radial acceleration changes sign, the $m = 1$ MRT-kink mode grows faster than the $m = 0$ MRT-sausage mode for shorter wavelengths ($\sim$1 mm) when there is a pre-seeded axial magnetic field.

The intricate interplay between the $m = 0$ and $m = 1$ modes, which also depends on the magnitude and sign of g, makes the interpretation of the helical structure observed by Awe *et al.*[12,13] and the apparent kink-like activities in Gomez *et al.*[14] difficult. Most questions on them remain unanswered. Among them include the sharpness of helical structures, the underlying reasons for the observed mode numbers (m, k), the role of initial seeding, the origin and maintenance of the helical structures, and their relation (if

any) to the kink-like mode that seems to have shown up at the final stage in the liner experiment of Gomez *et al.*[14] Our analysis does show that if helical perturbations are present on the liner surface, the axial magnetic field opens a window for the kink to grow instead of the sausage mode.

Despite the uncertainties, one puzzle on the experiment of Awe *et al.*,[12,13] namely, why the helical structures *opened* up (instead of very tightly wound up as the azimuthal magnetic field increases; see Fig. 4(a)) may be explained in terms of an *eigenmode* with a specific m and k. The axial wavenumber, k, is assumed to be constant. The frames in the experiment of Awe *et al.*,[12,13] occur over a narrow time window so this seems adequate. The pitch angle of the helix, ϕ, of the eigenmode is given by $\phi = \tan^{-1}(m/kR) \approx m/kR$, relating the values of ϕ(t2) and ϕ(t1) at different times t2 and t1: $\phi(t2) = \phi(t1) \times R(t1)/R(t2)$. For the Z-Machine Shot 2480, the measured (mean) values are $\phi(t1) = 16.4^\circ$, $a(t1) = 870\,\mu$m, $a(t2) = 365\,\mu$m. We then have, $R(t1) = a(t1) + \Delta = 870\,\mu\text{m} + 465\,\mu\text{m} = 1335\,\mu$m, and $R(t2) = 365\,\mu\text{m} + 465\,\mu\text{m} = 830\,\mu$m, where we have assumed that the liner thickness $\Delta = 465\,\mu$m remains unchanged throughout (see Fig. 4(b) and Awe *et al.*[12,13]). The predicted helix pitch angle at t2 is then $\phi(t2) = 16.4^\circ \times 1335/830 = 26.4^\circ$, which is quite close to the observed mean value of $\phi(t2) = 25.6^\circ$. Using this technique, the predicted value for $\phi(t2)$ in Shot 2481 is within the experimental uncertainties of the measured value also. This interpretation of the persistence of helical structures was motivated by the density wave theory that also used eigenmodes to explain the persistence of spiral structures in disk galaxies despite strong differential rotation.[23] Reproduction of the experimentally observed helical structures from simulations, without artificial seeding, has proved very challenging. 3D MHD simulations have required initial seeding of a helix to reproduce the observed helical structure; it has not simply arisen out of white noise.[13] Unfortunately, this seeding has also produced helical structure when no axial magnetic field is present which is not in line with experimental results. The sharpness of the helices and very specific mode numbers (in m and k) that were observed present the biggest challenge in comparing (unseeded) 3D simulations and experiments.

ACKNOWLEDGMENTS

This work was supported by DoE Award Nos. DE-SC0002590 and DE-SC0012328. Matt Weis was supported by the Sandia National Laboratories. Sandia National Laboratories is a multi-program laboratory managed and operated by Sandia Corporation, a wholly owned subsidiary of Lockheed Martin Corporation, for the U.S. Department of Energy's National Nuclear Security Administration under Contract No. DE-AC04-94AL85000.

[1]G. I. Taylor, Proc. R. Soc. London, Ser. A **201**, 192 (1950).
[2]M. Kruskal and M. Schwarzschild, Proc. R. Soc. London, Ser. A **223**, 348 (1954).
[3]S. Chandrasekhar, *Hydrodynamic and Hydromagnetic Stability* (Oxford University Press, London, United Kingdom, 1961), p. 429.
[4]E. G. Harris, Phys. Fluids **5**, 1057 (1962).
[5]A. B. Bud'ko, M. A. Liberman, A. L. Velikovich, and F. S. Felber, Phys. Fluids B **2**, 1159 (1990).
[6]D. D. Ryutov, M. S. Derzon, and M. K. Matzen, "The physics of fast Z pinches," Rev. Mod. Phys. **72**, 167 (2000).
[7]D. D. Ryutov and M. A. Dorf, Phys. Plasmas **21**, 112704 (2014).
[8]S. A. Slutz, M. C. Herrmann, R. A. Vesey, A. B. Sefkow, D. B. Sinars, D. C. Rovang, K. J. Peterson, and M. E. Cuneo, Phys. Plasmas **17**, 056303 (2010).
[9]D. B. Sinars, S. A. Slutz, M. C. Herrmann, R. D. McBride, M. E. Cuneo, K. J. Peterson, R. A. Vesey, C. Nakhleh, B. E. Blue, K. Killebrew, D. Schroen, K. Tomlinson, A. D. Edens, M. R. Lopez, I. C. Smith, J. Shores, V. Bigman, G. R. Bennett, B. W. Atherton, M. Savage, W. A. Stygar, G. T. Leifeste, and J. L. Porter, Phys. Rev. Lett. **105**, 185001 (2010).
[10]D. B. Sinars, S. A. Slutz, M. C. Herrmann, R. D. McBride, M. E. Cuneo, C. A. Jennings, J. P. Chittenden, A. L. Velikovich, K. J. Peterson, R. A. Vesey, C. Nakhleh, E. M. Waisman, B. E. Blue, K. Killebrew, D. Schroen, K. Tomlinson, A. D. Edens, M. R. Lopez, I. C. Smith, J. Shores, V. Bigman, G. R. Bennett, B. W. Atherton, M. Savage, W. A. Stygar, G. T. Leifeste, and J. L. Porter, Phys. Plasmas **18**, 056301 (2011).
[11]R. D. McBride, S. A. Slutz, C. A. Jennings, D. B. Sinars, M. E. Cuneo, M. C. Herrmann, R. W. Lemke, M. R. Martin, R. A. Vesey, K. J. Peterson, A. B. Sefkow, C. Nakhleh, B. E. Blue, K. Killebrew, D. Schroen, T. J. Rogers, A. Laspe, M. R. Lopez, I. C. Smith, B. W. Atherton, M. Savage, W. A. Stygar, and J. L. Porter, Phys. Rev. Lett. **109**, 135004 (2012).
[12]T. J. Awe, R. D. McBride, C. A. Jennings, D. C. Lamppa, M. R. Martin, D. C. Rovang, S. A. Slutz, M. E. Cuneo, A. C. Owen, D. B. Sinars, K. Tomlinson, M. R. Gomez, S. B. Hansen, M. C. Herrmann, J. L. McKenney, C. Nakhleh, G. K. Robertson, G. A. Rochau, M. E. Savage, D. G. Schroen, and W. A. Stygar, Phys. Rev. Lett. **111**, 235005 (2013).
[13]T. J. Awe, C. A. Jennings, R. D. McBride, M. E. Cuneo, D. C. Lamppa, M. R. Martin, D. C. Rovang, D. B. Sinars, S. A. Slutz, A. C. Owen, K. Tomlinson, M. R. Gomez, S. B. Hansen, M. C. Herrmann, M. C. Jones, J. L. McKenney, G. K. Robertson, G. A. Rochau, M. E. Savage, D. G. Schroen, and W. A. Stygar, Phys. Plasmas **21**, 056303 (2014).
[14]M. R. Gomez, S. A. Slutz, A. B. Sefkow, D. B. Sinars, K. D. Hahn, S. B. Hansen, E. C. Harding, P. F. Knapp, P. F. Schmit, C. A. Jennings, T. J. Awe, M. Geissel, D. C. Rovang, G. A. Chandler, G. W. Cooper, M. E. Cuneo, A. J. Harvey-Thompson, M. C. Herrmann, M. H. Hess, O. Johns, D. C. Lamppa, M. R. Martin, R. D. McBride, K. J. Peterson, J. L. Porter, G. K. Robertson, G. A. Rochau, C. L. Ruiz, M. E. Savage, I. C. Smith, W. A. Stygar, and R. A. Vesey, Phys. Rev. Lett. **113**, 155003 (2014).
[15]Y. Y. Lau, J. C. Zier, I. M. Rittersdorf, M. R. Weis, and R. M. Gilgenbach, Phys. Rev. E **83**, 066405 (2011).
[16]P. Zhang, Y. Y. Lau, I. M. Rittersdorf, M. R. Weis, R. M. Gilgenbach, D. Chalenski, and S. Slutz, Phys. Plasmas **19**, 022703 (2012).
[17]J. C. Zier, R. M. Gilgenbach, D. A. Chalenski, Y. Y. Lau, D. M. French, M. R. Gomez, S. G. Patel, I. M. Rittersdorf, A. M. Steiner, M. Weis, P. Zhang, M. Mazarakis, M. E. Cuneo, and M. Lopez, Phys. Plasmas **19**, 032701 (2012).
[18]M. R. Weis, P. Zhang, Y. Y. Lau, I. M. Rittersdorf, J. C. Zier, R. M. Gilgenbach, M. H. Hess, and K. J. Peterson, Phys. Plasmas **21**, 122708 (2014).
[19]J. M. Koning, G. D. Kerbel, and M. M. Marinak, "The Hydra Magnetohydrodynamics Package," APS-DPP (2009); M. M. Marinak, G. Kerbel, N. Gentile, O. Jones, D. Munro, S. Pollaine, T. R. Dittrich, and S. W. Haan, Phys. Plasmas **8**, 2275 (2001).
[20]P. M. Bellan, *Fundamentals of Plasma Physics* (Cambridge University Press, 2006).
[21]K. J. Peterson, D. B. Sinars, E. P. Yu, M. C. Herrmann, M. E. Cuneo, S. A. Slutz, I. C. Smith, B. W. Atherton, M. D. Knudson, and C. Nakhleh, Phys. Plasmas **19**, 092701 (2012).
[22]K. J. Peterson, E. P. Yu, D. B. Sinars, M. E. Cuneo, S. A. Slutz, J. M. Koning, M. M. Marinak, C. Nakhleh, and M. C. Herrmann, Phys. Plasmas **20**, 056305 (2013).
[23]C. C. Lin and F. H. Shu, Astrophys. J. **140**, 646 (1964); Y. Y. Lau, C. C. Lin, and J. W.-K. Mark, Proc. Natl. Acad. Sci. U.S.A. **73**, 1379 (1976); G. Bertin, *Dynamics of Galaxies*, 2nd ed. (Cambridge University Press, New York, 2014).